ISSN (Print) 1226-1750
ISSN (Online) 2233-6656
Journal of Magnetics 22(4), 570-578 (2017) https://doi.org/10.4283/JMAG.2017.22.4.570

Study on Feasibility for Artificial Intelligence (AI) Noise Reduction Algorithm with Various Parameters in Pediatric Abdominal Radio-Magnetic Computed Tomography (CT)

Seung Hun Kim, Kanghyen Seo, Seong-Hyeon Kang, Seyoung Bae, Hyeng Ju Kwak, Ji Woo Hong, Yoonji Hwang, Sung Mo Kang, Hye Ran Choi, Ga Yun Kim, and Youngjin Lee*

Department of Radiological Science, Eulji University, 553, Sanseong-daero, Sujeong-gu, Seongnam-si, Gyeonggi-do 13135, Republic of Korea

(Received 29 September 2017, Received in final form 8 November 2017, Accepted 13 November 2017)

The importance of radiation-based images has been increasing due to their ability to provide rapid diagnosis and facilitate treatment of lesions. Among them, the frequency of examination using computed tomography (CT) has been increasing because of this technique's fast examination time and high diagnostic power. However, although the criteria for screening have been presented based on many previous studies on the CT exposure dose for adults, the criteria for children remain inadequate. Especially, relaxing the conditions to reduce the exposure dose of CT will lead to generation of noises. To address this problem, many noise removal algorithms have been developed. Among developed algorithms, a particularly strong interest has been focused on deep learning methods, which are a sort of artificial intelligence (AI)-based machine learning. Therefore, the present study aimed to develop a noise removal algorithm using the Gaussian Mixture Model (GMM), an AI-based deep learning method, and to apply the algorithm to pediatric abdominal CT so that to evaluate the usefulness of the approach. PMMA phantoms with different diameters of 12, 16, 20, 24, and 32 cm, which can express pediatric abdomen, were manufactured and used. To evaluate dose and image quality, the tube current was fixed to 200 mAs and the tube voltage was changed from 80 to 120, and 140 kVp; thereafter, the tube voltage was fixed to 120 kVp and the tube currents were changed from 50 to 100, 150, 200, and 250 mAs. According to the results, CTDIw showed a tendency to increase alongside with increases in the tube voltage and the tube currents, while noise decreased proportionally. In addition, the contrast decreased as the tube voltage increased, but was shown to be almost unrelated to the tube currents. Finally, the excellent CNRD result was measured in lowest exposure condition at 80 kVp and 50 mAs. Also, the average of CNRD with AI noise reduction algorithm was 1.6-4.2 times higher than before the application. In conclusion, the doses and characteristics of the pediatric abdominal CT scan according to various image acquisition conditions could be successfully identified and the efficiency of the AI noise removal algorithm developed in the present study was demonstrated.

Keywords : pediatric abdominal computed tomography (CT), Artificial intelligence (AI)-based machine learning, deep learning, image processing, noise reduction algorithm, dose and image quality evaluation

1. Introduction

The importance of images obtained using radiation for diagnosis and treatment of patients has been rapidly increasing. Consequently, numerous studies have been carried out and, as a result, the radiation image technology and medical image devices have made a great progress. Among them, the use and interest of computed tomography (CT) have recently increased in terms of the management of the high medical exposures of CT scanning. In particular, due to the occurrence of a series of nuclear accidents–ranging from the Chernobyl accident in the past to the recent Fukushima nuclear accident–patients' wariness against radiation has increased, making it essential to continue research on dose reduction [1]. However, in general, if the dose is reduced when CT images are acquired, although safety against exposure will increase, many noises will occur, leading to a deterioration of image quality.

To amend the situation, many studies on noise reduction

*Corresponding author: Tel: +82-31-740-7264
Fax: +82-31-740-7351, e-mail: radioyoungj@gmail.com

algorithm have been conducted. In the beginning, methods using the mean value of the region of interest (ROI), such as median filters, were used. However, this approach yielded a shortcoming of the removal of information alongside with noises. To address this problem, various techniques have been developed, such as wavelet transform, which preserves and processes spatial information when the information is transformed from the spatial domain to the frequency domain and total variation (TV) that removes noises using probabilistic distribution obtained through numerical formulas, taking advantage of the fact that diverse arithmetic operations have become possible due to the development of computers [2-4].

Recently, as following the advent of AlphaGo, interest in artificial intelligence (AI) has been increased, attempts have been made to combine CT with AI. In the field of medical technology, a domain of AI called machine learning, which is an algorithm to learn information in existing data to perform works on new data, has received particular research attention, and out of it, deep learning has emerged. Deep learning is a method of enhancing the learning ability of neural networks by piling up artificial neural networks. Early artificial neural networks were supervised learning systems for which the data containing correct answers should be provided by experts for learning. However, as learning was implemented with large amounts of data, overfitting, which is learning even unnecessary information, has occurred. To complement the above, the restricted Boltzmann machine (RBM) that learns to follow the Boltzmann distribution and the drop out system that omits variables in the networks have been developed, so that the problem of overfitting was improved. In addition, unsupervised learning in which correct answers are not given to learning data has also become possible. Therefore, studies on noise reduction algorithms have been actively conducted in diverse ways to improve image quality [5, 6].

On the other hand, apart from the development of noise reduction algorithms, although examination standards have been presented through continuous studies to prepare countermeasures against the high exposures of CT examination in the case of adults, consideration of exposure is insufficient in the case of pediatric CT. This is so because not only potential risks are high in children (since children are more sensitive as compared to adults), but also the overall examination standards have not been accurately defined. In particular, few studies have been conducted on the optimization of image quality for dose reduction in pediatric abdominal CT scanning. Therefore, in the present study, CT phantoms capable of simulating the abdomens of children will be manufactured to acquire CT images while changing kVp and mAs; the dose and image quality will be evaluated, and the developed AI based noise reduction algorithm will be applied in order to prove the usefulness.

The structure of this paper is as follows: in Section 2, we describe our noise reduction algorithm with AI in detail and experimental conditions including phantom manufacturing. In Section 3, the noise reduction algorithm is applied to the phantom imaged obtained through the experiment to compare the dose, image quality using contrast-to-noise ratio (CNR), and contrast-to-noise ratio and dose (CNRD) of each phantom images with each other. Finally, in Section 4, based on the contents compared as described above, criteria for pediatric abdominal CT scanning are proposed.

2. Materials and Methods

2.1. Noise reduction algorithm with AI

Noise reduction algorithms are algorithms to remove the noises that inevitably occur in images and have the following basic equation (see Eq. (1)):

$$D = Tx + \rho \tag{1}$$

where D is the acquired images, Tx is the clean images, and ρ is the noise. Noise reduction algorithms are divided into the methods that find and remove ρ and those that directly obtain Tx without removing ρ. The deep learning method used here will employ a noise reduction algorithm that will directly obtain Tx. The Gaussian Mixture Model (GMM) will be used as a method of obtaining Tx to get the originally clean image quality of the images and to execute the noise reduction algorithm [7].

The GMMs made assuming an appropriate probability density function in order to know the data distribution characteristics are called probability models. Among them, the Gaussian probability distribution is the most widely used model. However, the Gaussian probability distribution has the limitation of being capable of using only the data in unimodal forms around the mean. Therefore, the GMM is being used. When M GMM filters are used in images, the equation is as follows (see Eq. (2)):

$$p(x|\theta) = \Sigma_{i=1}^{M} p(x|\omega_i, \theta_i)\ P(\omega_i) \tag{2}$$

where $p(x|\omega_i, \theta_i)$ is the Gaussian probability density function, θ_i is the parameters of the probability density function, which is the ith component that are mean and covariance matrix, and ω_i refers to the ith random variable. $P(\omega_i)$ refers to the relative importance of the ith component in the entire mixed probability density function and should satisfy $0 \le P(\omega_i) \le 1$ and $\Sigma_{i=1}^{M} P(\omega_i) = 1$.

Then, the Gaussian probability density that constitutes the jth component is as follows (see Eq. (3)):

$$p(x_n|\omega_j,\ \theta) = p(x_n|\mu_j,\ \sigma_j^2) \tag{3}$$

In Eq. (3), μ_j is mean and σ_j^2 is variance. The mixed probability that combined M pieces of these individual components is as follows (see Eq. (4)):

$$p(x_n|\theta) = \Sigma_{i=1}^{M}\ p(x_n|\mu_j,\ \sigma_j^2)P(\omega_J) \tag{4}$$

When GMM is used, Z, i.e. a hidden random variable such as maximum likelihood function, should be estimated. To find the best estimate through repetitive operations, the EM algorithm is used for the estimation. The EM algorithm is divided into E-step and M-step. First, in the E-step (Expectation - step), the expected value of the hidden random variable is calculated so that it can be used instead of the observed value. In the M-step (Maximization-step), the value of the parameter that maximizes the likelihood function is searched using the observed data x and the expected value of the hidden random variable. The solving process is as follows: first, the values of the parameters are arbitrarily determined in the E-step and then the expected value E [Z] of the hidden variable Z is calculated using the probability model determined by the determined parameters. For each observed data x_i, the probability for the value Z_i of the hidden random variable to (1,0) and the probability to be (0,1) should be calculated. Using parameter values, the probabilities can be calculated as follows (see Eq. (5)):

$$P(\omega_i = 1|x_i,\ \mu_i,\ \sigma_j^2) = p(\omega_j|x_i,\ \theta) = \frac{p(x_n|\mu_j,\ \sigma_j^2)p(\omega_j)}{p(x_n|\theta)} \tag{5}$$

The M-step is a step of a new estimating the parameter using the value of the hidden variable z calculated in the E-step. Although the groups from which individual data x_i have come cannot be exactly known, the parameter can be calculated as follows. In Eq. (5), if the partial differentiation is applied to find the value of μ_j that is 0, the following equation can be obtained (see Eq. (6)):

$$\mu_j = \frac{\Sigma_{n=1}^{N} p(\omega_j|x_n)x_n}{\Sigma_{n=1}^{N} p(\omega_j|x_n)} \tag{6}$$

Since $P(\omega_j)$ means the ratio of the jth group in the entire data, if the equation for partial differentiation is used in the above method so that the value becomes 0 considering $P(Z=j|x_i)$ the following equation can be obtained (see Eq. (7)):

$$P(\omega_j) = \frac{1}{N}\Sigma_{i=1}^{N} P(\omega_j|x_n) \tag{7}$$

When M-step has been implemented, a new parameter modified from the previous parameter is obtained. Using the parameter, the E-step to calculate the expected value of the hidden variable z or probability value can be implemented again. The M-step and E-step are repeated so that to estimate a more accurate parameter. Figure 1 shows a flow chart of the overall process.

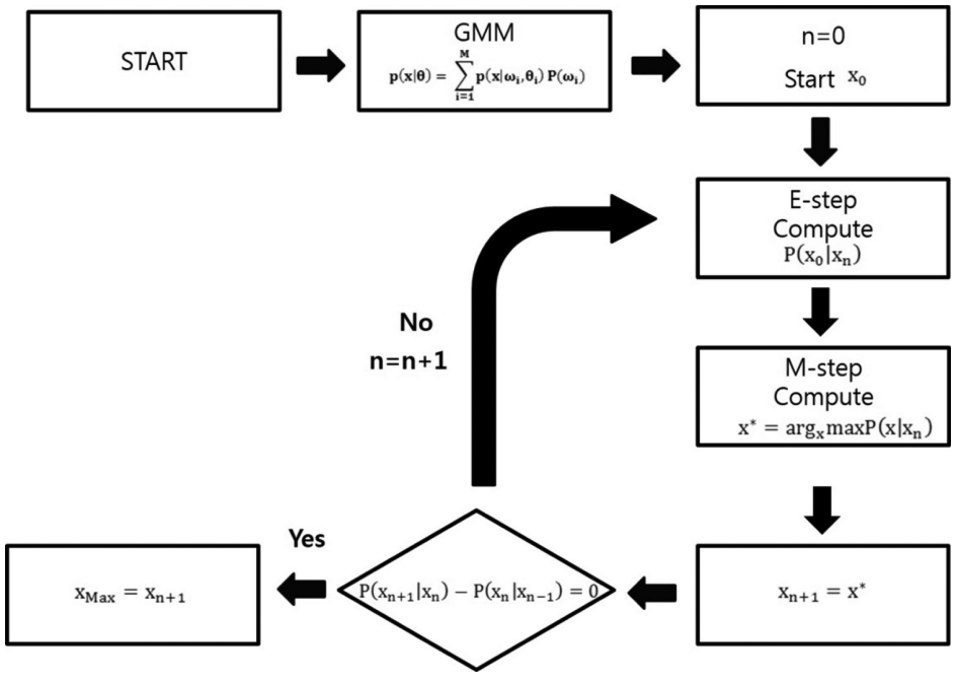

Fig. 1. The schematic diagram for deep learning flow chart using Gaussian Mixture Model (GMM) algorithm.

Fig. 2. (Color online) The photo of (a) SOMATOM Definition AS CT device used in experiment and (b) manufactured phantom with different diameters (12, 16, 20, 24, and 32 cm).

2.2. Equipment and experimental condition

Figure 2 shows the CT equipment and phantoms used in the experiment. The CT equipment is SOMATOM Definition AS with 128 slice (Siemens). PMMA phantoms with diameters of 12, 16, 20, 24, and 32 cm, which can simulate pediatric abdomen, were manufactured. The tube current was fixed to 200 mAs and the tube voltage was changed from 80 to 120 and 140 kVp; thereafter, the tube voltage was fixed to 120 kVp and the tube currents were changed from 50 to 100, 150, 200, 250, and 300 mAs to conduct the experiment.

2.3. Evaluation method

We used CTDIw, CNR and CNRD to evaluate the dose and image quality. The dose was examined through CTDIw; CNR was used to evaluate the image quality and CNRD values were obtained to examine the correlation between the dose and image quality. CTDIw represents the average dose in the scan plane of Perspex phantoms. Figure 3 shows the method to obtain CTDIw [8]. The average dose of the entire phantoms is shown by the value obtained by adding 1/3 of the dose shown in the dosimeter located in the center and 2/3 of the average value of the doses shown in the dosimeters located on the edge.

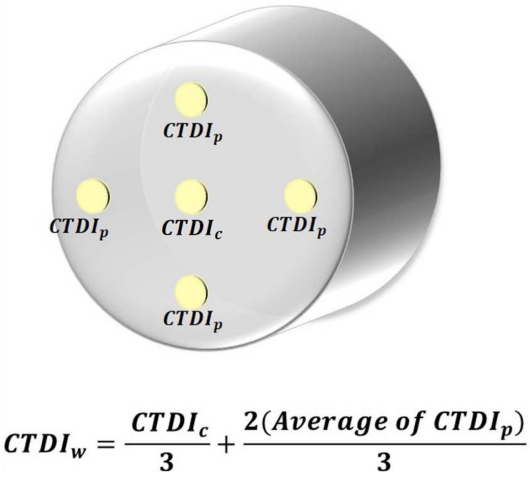

$$CTDI_w = \frac{CTDI_c}{3} + \frac{2(Average\ of\ CTDI_p)}{3}$$

Fig. 3. (Color online) The schematic diagram of method to obtain CTDIw. CTDIw is a weighted average of the CTDI at the center and periphery of the phantom and represents the average radiation dose over the X and Y direction.

We used CNRD to evaluate the relationship between the image quality and the dose and to derive the optimized value. The equation to obtain CNRD is as follows:

$$\mathrm{CNRD} = \frac{\mathrm{CNR}}{\sqrt{\mathrm{Dose}}} \tag{8}$$

3. Results

Figure 4 shows the CTDIw measured by phantom diameter while changing kVp and mAs. As shown in Fig. 4(a), the CTDIw values were measured as 21.15, 63.17, and 83.55 mGy at 80, 120, and 140 kVp, respectively, in the smallest-diameter phantom. In the largest-diameter phantom, the values were measured as 10.05, 24.80, and 32.05 mGy at 80, 120, and 140 kVp, respectively. In general, the CTDIw values measured at five diameters almost linearly increased as kVp increased and it was identified that the smaller the diameter, the larger the amounts of increase. In addition, as can be seen in Fig. 4(b), in the smallest-diameter phantom, the CTDIw values were measured as 15.91, 30.17, 47.35, 63.17, 75.99 and 93.19 mGy at 50, 100, 150, 200, 250 and 300 mAs, respectively. In the largest-diameter phantom, the

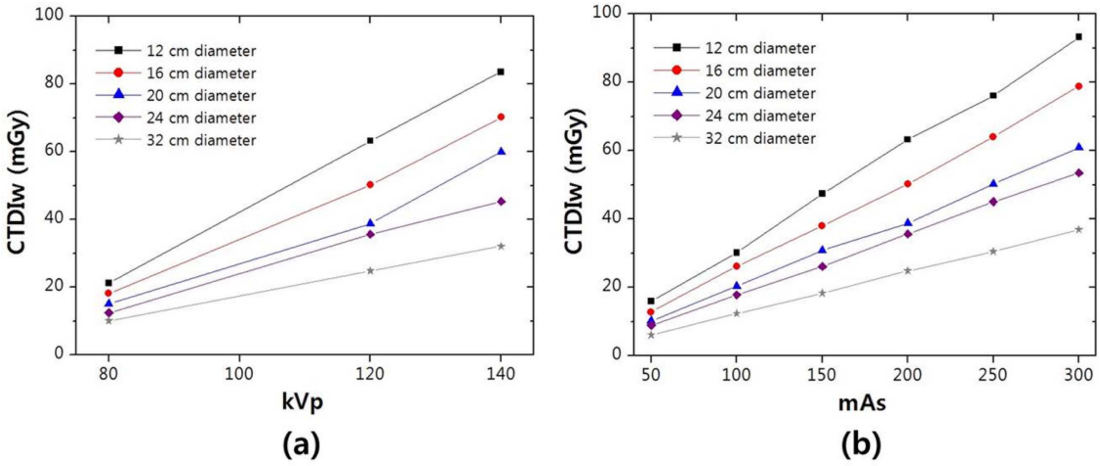

Fig. 4. (Color online) The acquired dose results as a function of (a) kVp and (b) mAs with various pediatric abdominal phantom diameters.

values were measured as 6.08, 12.35, 18.35, 24.8, 30.5, and 36.91 mGy at 50, 100, 150, 200, 250, and 300 mAs respectively. In this case, CTDIw increased as mAs increased and that the smaller the diameter, the larger the amounts of increase in all five diameters.

Figure 5 shows noise values a ccording to the changes

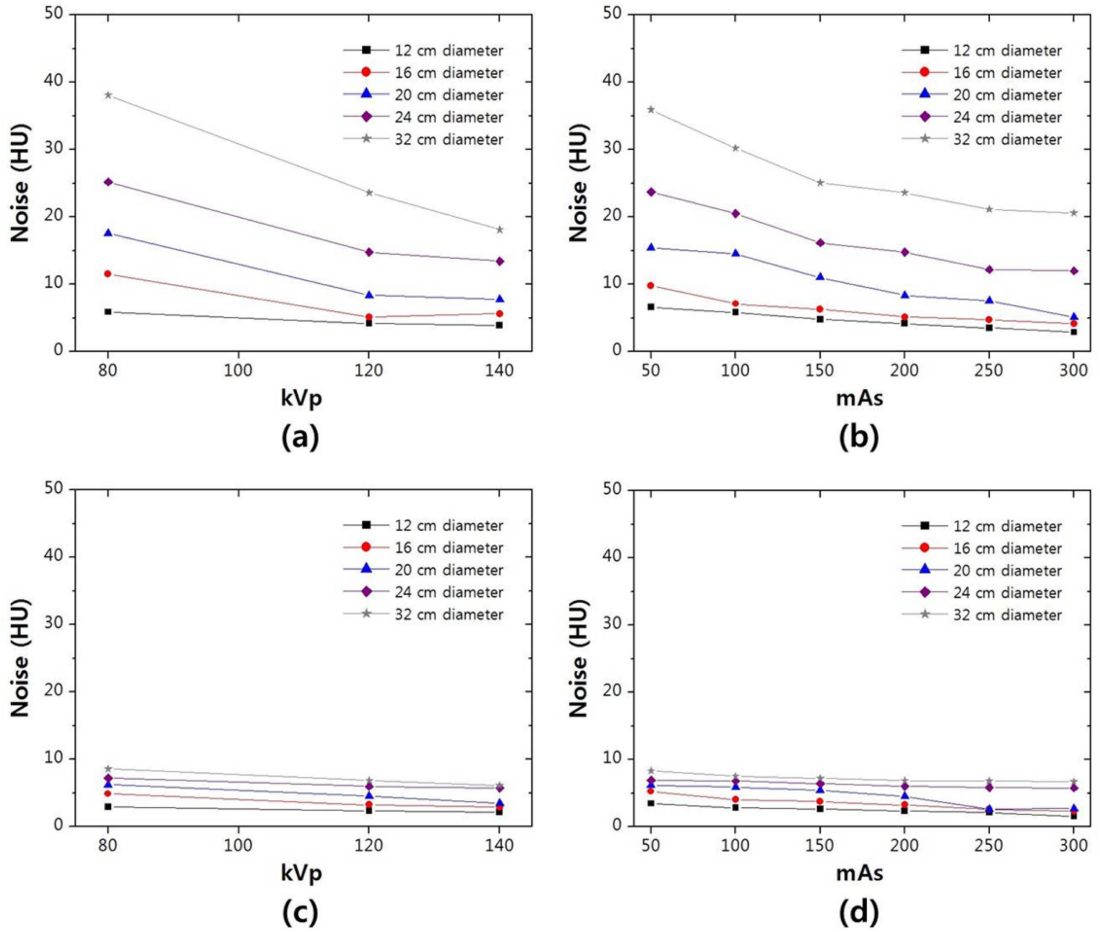

Fig. 5. (Color online) The acquired noise results (HU) as a function of (a) kVp and (b) mAs with various pediatric abdominal phantom diameters before applying the noise reduction algorithm. Also, the acquired noise results as a function of (c) kVp and (d) mAs with various pediatric abdominal phantom diameters after applying the noise reduction algorithm.

in the tube voltage and tube current before and after applying the developed noise reduction algorithm. Figures 5(a) and (b) show graphs of the noises (Hounsfield Unit; HU) measured before applying the noise reduction algorithm; Figures 5(c) and (d) show graphs of the noises measured after applying the noise reduction algorithm. As can be seen in Fig. 5(a), in the smallest-diameter phantom, the noise values were measured as 5.89, 4.18, and 3.87 HU at 80, 120, and 140 kVp, respectively. In the largest-diameter phantom, the values were measured as 38.09, 23.58, and 18.1 HU at 80, 120, and 140 kVp, respectively, indicating that the noise decreased as the tube voltage increased. When the above results were reconstructed with the noise reduction algorithm, the noise values decreased as the tube voltage increased. In the smallest-diameter phantom, the values were 2.89, 2.35, and 2.11 HU at 80, 120, and 140 kVp, respectively, and, in the largest-diameter phantom, the values were 8.55, 6.85, and 6.10 HU at 80, 120, and 140 kVp, respectively. Therefore, it was identified that, compared to before the application, the noises decreased for 1.7-4.4 times when the noise reduction algorithm was applied (see Fig. 5(c)). In addition, as can be seen in Fig. 5(b), in the smallest-diameter phantom, the noise values were measured as 6.59, 5.83, 4.78, 4.18, 3.51, and 2.87 HU at 50, 100, 150, 200, 250, and 300 mAs, respectively and, in the largest-diameter phantom, the noise values were measured as 35.89, 30.19, 25.03, 23.58, 21.12, and 20.58 HU at 50, 100, 150, 200, 250, and 300 mAs, respectively, indicating that the noises decreased as the tube current increased. When the above results were reconstructed with the noise reduction algorithm, the noise values decreased from 3.44 to 2.81, 2.63, 2.35, 2.09, and 1.51 HU in the smallest-diameter phantom and from 8.31 to 7.5, 7.18, 6.85, 6.78, and 6.72 HU in the largest-diameter phantom as the tube current increased from 50 to 100, 150, 200, 250, and 300 mAs. Therefore, as compared to before the application, the noises decreased for 1.6-4.3 times when the noise reduction algorithm was applied, indicating that when the noise reduction algorithm was applied, quite some noises were

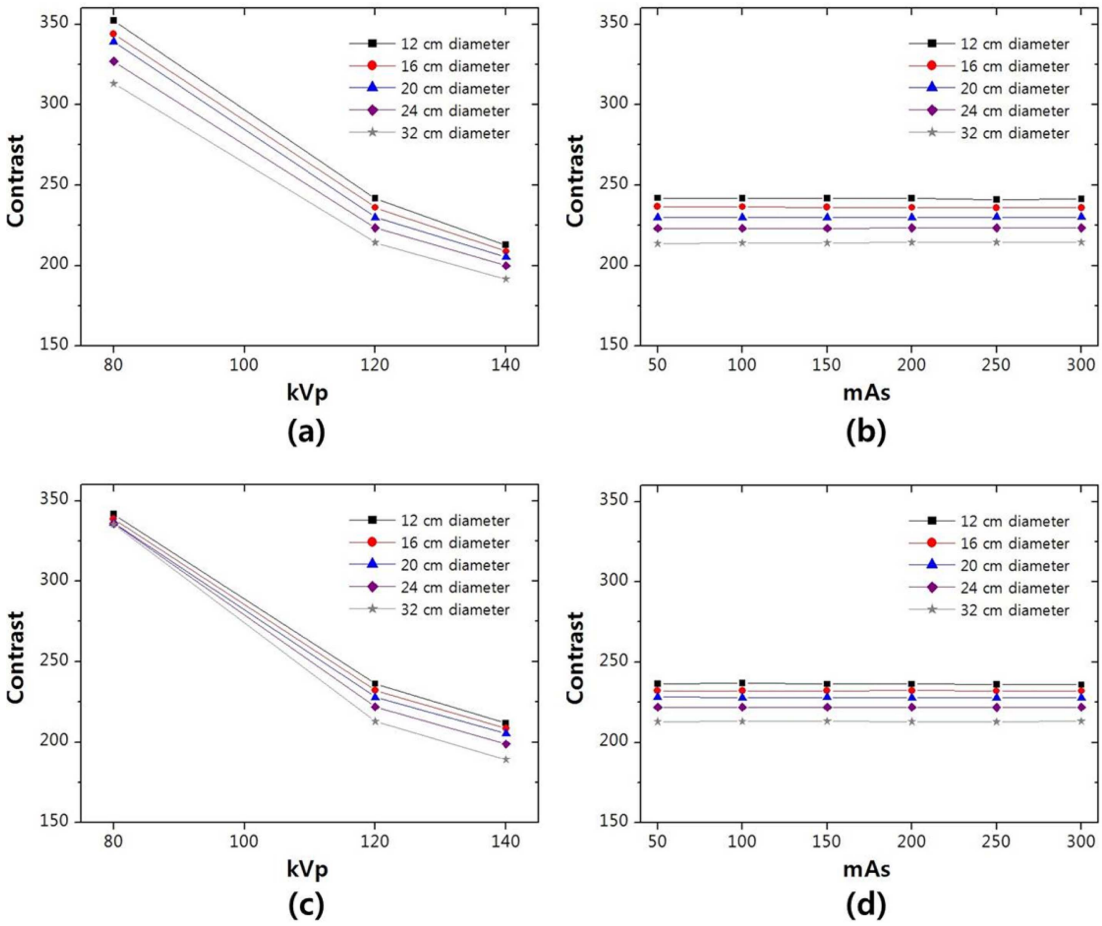

Fig. 6. (Color online) The acquired contrast results as a function of (a) kVp and (b) mAs with various pediatric abdominal phantom diameters before applying the noise reduction algorithm. Also, the acquired contrast results as a function of (c) kVp and (d) mAs with various pediatric abdominal phantom diameters after applying the noise reduction algorithm.

removed in all conditions.

Figure 6 shows contrast values according to the changes in the tube voltage and tube current before and after application of the developed noise reduction algorithm. Figures 6(a)-(b) shows graphs of contrast before the application of the noise reduction algorithm; Figures 6 (c)-(d) shows graphs of contrast after the application of the noise reduction algorithm. As can be seen in Fig. 6 (a), in the smallest-diameter phantom, the contrast was measured as 352.21, 241.70, and 212.72 at 80, 120, and 140 kVp, respectively and, in the largest-diameter phantom, the contrast was measured as 313.1, 214.3, and 191.6 at 80, 120, and 140 kVp, respectively, indicating that contrast decreased as the tube voltage increased. In the case of Fig. 6(b), in the smallest-diameter phantom, the contrast was measured for 241 at 50, 100, 150, 200, 250 and 300 mAs and, in the largest-diameter phantom, the contrast was measured for 214 at all current values, indicating that contrast is not significantly related to tube current and that contrast was not changed very much after the application of the noise reduction algorithm as compared to before the application.

Figure 7 shows a graph regarding CNRD drawn based on the measured CTDIw, noise, and contrast as described above. Figure 7(a)-(b) shows the graphs of CNRD before the application of the noise reduction algorithm and Fig. 7(c)-(d) shows the graphs of CNRD after the application. As shown in Fig. 7(a), in the smallest-diameter phantom, CNRD was measured as 13.0, 7.2, and 6.0 at 80, 120, and 140 kVp, respectively, and in the largest-diameter phantom, CNRD was measured as 2.5, 1.9, and 1.8 at 80, 120, and 140 kVp, respectively, indicating that CNRD decreased as the tube voltage increased. When the above results were reconstructed with the noise reduction algorithm, in the smallest-diameter phantom, CNRD was measured as 25.6, 12.6 and 10.9 at 80, 120, and 140 kVp, respectively, and in the largest-diameter phantom, CNRD was measured as 12.3, 5.8, and 5.4 at 80, 120, and 140 kVp, respectively, indicating that CNRD decreased as the tube voltage increased and that CNRD increased for 1.7-4.9 times after

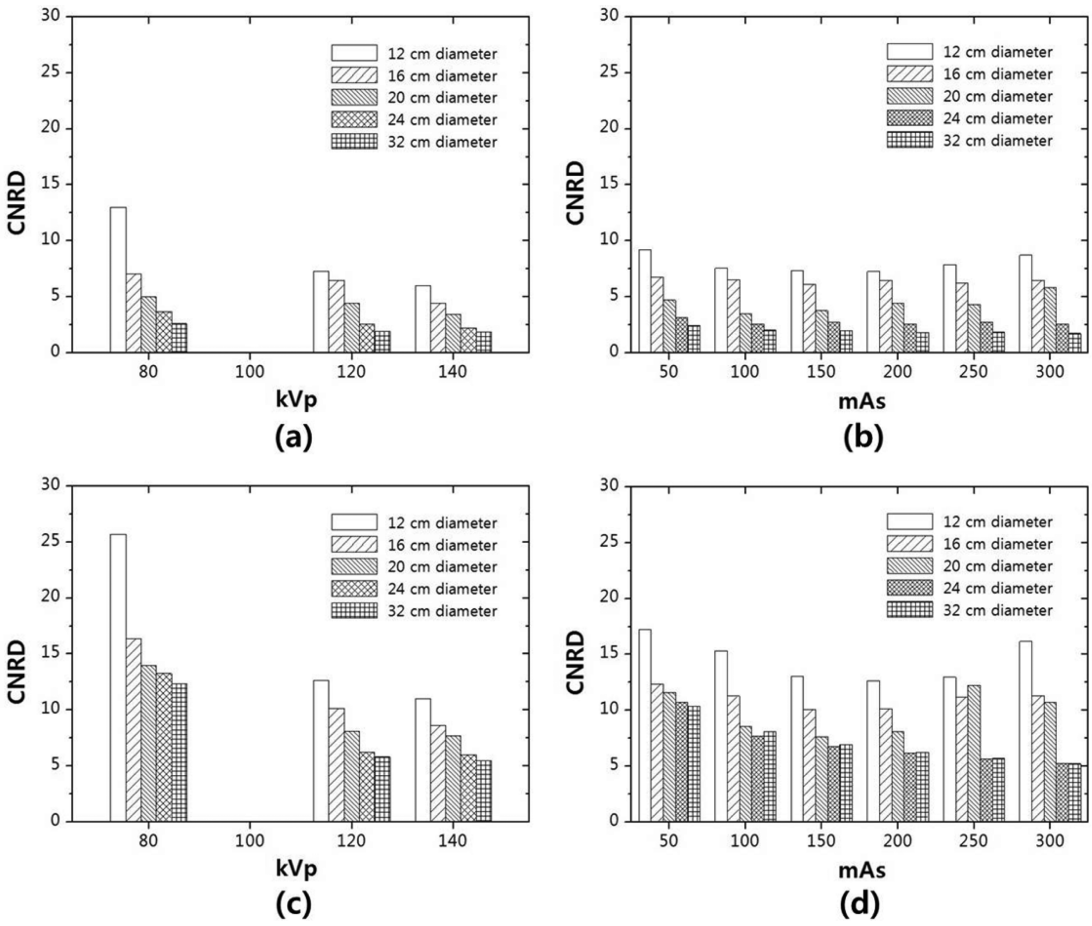

Fig. 7. The acquired CNRD results as a function of (a) kVp and (b) mAs with various pediatric abdominal phantom diameters before applying the noise reduction algorithm. Also, the acquired CNRD results as a function of (c) kVp and (d) mAs with various pediatric abdominal phantom diameters after applying the noise reduction algorithm.

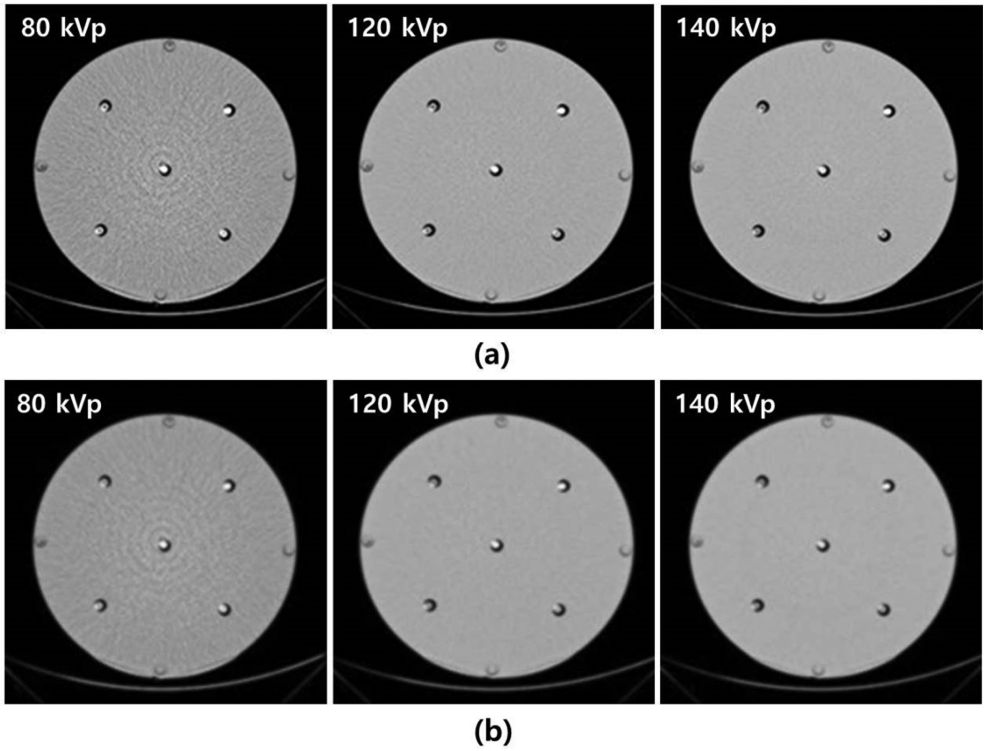

Fig. 8. The example of acquired 32 cm phantom diameter images using 80, 120, and 140 kVp with (a) before and (b) after applying the noise reduction algorithm.

the application of the noise reduction algorithm as compared to before the application (see Fig. 7(c)). On the other hand, unlike in Fig. 7(a), as shown in Fig. 7(b), in the smallest-diameter phantom, CNRD was measured as 9.2, 7.5, 7.3, 7.2, 7.8, and 8.7 at 50, 100, 150, 200, 250, and 300 mAs, respectively and in the largest-diameter phantom, CNRD was measured as 2.4, 2.0, 1.9, 1.8, 1.8, and 1.7 at 50, 100, 150, 200, 250, and 300 mAs, indicating that, unlike in the results following changes in kVp, CNRD did not change according to mAs. When the above was reconstructed with the noise reduction algorithm, in the smallest-diameter phantom, CNRD was measured as 17.2, 15.3, 13.0, 12.6, 12.9, and 16.1 at 50, 100, 150, 200, 250, and 300 mAs, respectively, and in the largest-diameter phantom, CNRD was measured as 10.3, 8.0, 6.9, 6.2, 5.6, and 5.2 at 50, 100, 150, 200, 250, and 300 mAs, respectively, indicating that, as compared to before the application, CNRD increased for 1.6-4.2 times after the application of the noise reduction algorithm; however, the differences were not consistent (see Fig. 7(d)). The above can be attributed to occurrence of errors due to variations in the tube current examination time and consistent results can be obtained by increasing the number of times of experiments and obtaining average values. Consequently, both before and after the application of the noise reduction algorithm, in phantoms of all diameters, higher CNRD values could be obtained when kVp and mAs were lower.

Figure 8 shows the images of the 32 cm phantom diameter taken at 80, 120, and 140 kVp conditions before and after the application of the noise reduction algorithm.

4. Discussion

In the present study, we developed CTDI phantoms for pediatric abdomens, acquired CT images under various kVp and mAs conditions, and developed and applied a noise reduction algorithm to compare the dose and image quality before and after application.

Our results demonstrate that the dose increased as the tube voltage and the tube current increased and the diameter of phantoms decreased, while noises decreased as the tube voltage and the tube current increased and the diameter of phantoms decreased. In addition, contrast decreased as the tube voltage and phantom diameter increased, but was not much affected by the changes in the tube current.

Based on the CNRD results coupled with the results outlined above, we demonstrate that the proposed AI based noise reduction algorithm is more advantageous when more noises are generated, and, finally, the most

efficient resultant value could be obtained in the lowest condition.

5. Conclusion

In conclusion, in the present study, we proved the usefulness of the AI-based noise reduction algorithm and identified the optimal protocol for pediatric abdominal examination. In further research, we will model phantoms for not only the abdomen, but also for diverse regions to present an optimal protocol for the overall pediatric CT scan.

Acknowledgment

This research was supported by the National Research Foundation of Korea (NRF-2016R1D1A1B03930357) and the Korea Foundation for the Advancement of Science & Creativity (KOFAC) grant funded by Ministry of Education (MOE). Seung Hun Kim and Kanghyen Seo equally contributed to this work.

References

[1] T. W. Bowyer, S. R. Biegalski, M. Cooper, P. W. Eslinger, D. Haas, J. C. Hayes, H. S. Miley, D. J. Strom, and V. Woods, J. Environ. Radio. **102**, 681 (2011).
[2] C. M. Chen, Y. Y. Lin, M. Y. Hsu, C. F. Hung, Y. L. Liao, and H. Y. Tasi, Euro. J. Radio. **85**, 1666 (2016).
[3] C. R. Vogel and M. E. Oman, SIAM J. Scientific Computing **17**, 227 (1996).
[4] K. Seo, S. H. Kim, S. H. Kang, J. Park, C. L. Lee, and Y. Lee, J. Magn. **21**, 593 (2016).
[5] S. H. Kim, K. Seo, S. H. Kang, J. H. Kim, W. H. Choi, and Y. Lee, J. Magn. **22**, 55 (2017).
[6] S. Wang and R. M. Summers, Med. Image Anal. **16**, 933 (2012).
[7] J. Xu, L. Zhang, W. Zuo, D. Zhang, and X. Feng, The IEEE International Conference on Computer Vision (2015) pp 244-252.
[8] C. L. Lee, H. J. Kim, H. C. Yong, H. M. Cho, J. Y. Jung, H. S. Park, and A. R. Yu, J. Korean Phys. Soc. **54**, 1702 (2009).